



Twisted plasma waves driven by twisted ponderomotive force

Yin Shi¹ , David R Blackman², Robert J Kingham³, and Alexey Arefiev²

¹Department of Plasma Physics and Fusion Engineering, University of Science and Technology of China, Hefei 230026, China;

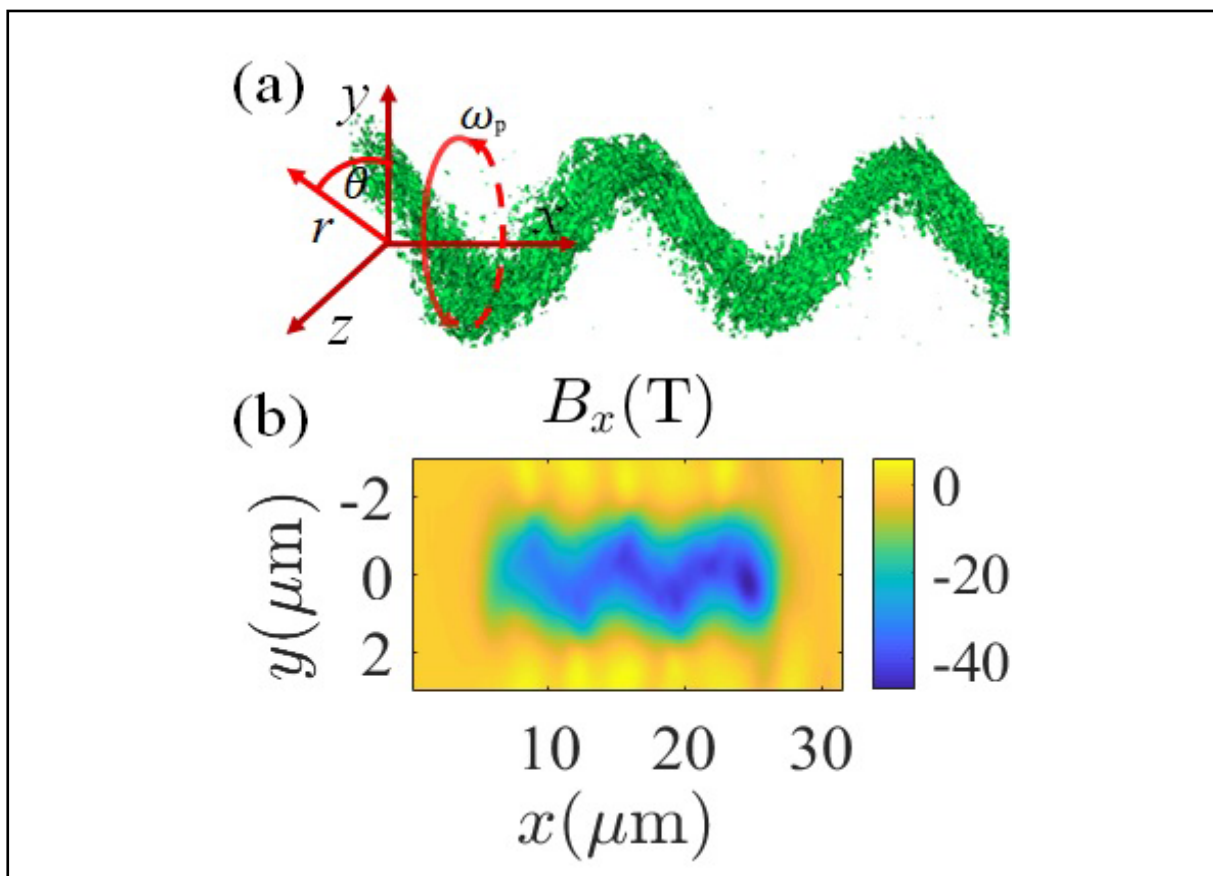
²Department of Mechanical and Aerospace Engineering, University of California at San Diego, CA 92093, USA;

³Blackett Laboratory, Imperial College London, London SW7 2AZ, UK

 Correspondence: Yin Shi, E-mail: shiyin@ustc.edu.cn

© 2023 The Author(s). This is an open access article under the CC BY-NC-ND 4.0 license (<http://creativecommons.org/licenses/by-nc-nd/4.0/>).

Graphical abstract



Twisted plasma waves driven by twisted ponderomotive force. (a) A 3D view of the electron density deviation in the plasma wave driven by twisted ponderomotive force, simulated using the EPOCH PIC code. (b) The distribution of longitudinal magnetic field at $z = 0$.

Public summary

- The plasma waves can be in a twisted mode when it is driven by twisted ponderomotive force.
- With beating of co-propagating Laguerre-Gaussian (LG) orbital angular momentum (OAM) laser beams with different frequencies and also different twist indices, twisted ponderomotive force can be got.
- A new magnetic field generation mechanism in underdense plasmas due to plasma waves is clarified in this study.

Twisted plasma waves driven by twisted ponderomotive force

Yin Shi¹ ✉, David R Blackman², Robert J Kingham³, and Alexey Arefiev²

¹Department of Plasma Physics and Fusion Engineering, University of Science and Technology of China, Hefei 230026, China;

²Department of Mechanical and Aerospace Engineering, University of California at San Diego, CA 92093, USA;

³Blackett Laboratory, Imperial College London, London SW7 2AZ, UK

✉Correspondence: Yin Shi, E-mail: shiyin@ustc.edu.cn

© 2023 The Author(s). This is an open access article under the CC BY-NC-ND 4.0 license (<http://creativecommons.org/licenses/by-nc-nd/4.0/>).



Cite This: *JUSTC*, 2023, 53(1): 3 (7pp)



Read Online

Abstract: We present the results of twisted plasma waves driven by twisted ponderomotive force. With the beating of two, co-propagating, Laguerre-Gaussian (LG) orbital angular momentum (OAM) laser pulses with different frequencies and also different twist indices, we can obtain the twisted ponderomotive force. Three-dimensional particle-in-cell simulations are used to demonstrate the twisted plasma waves driven by lasers. The twisted plasma waves have an electron density perturbation with a helical rotating structure. Different from the predictions of the linear fluid theory, the simulation results show a nonlinear rotating current and a static axial magnetic field. Along with the rotating current is the axial OAM carried by particles in the twisted plasma waves. A detailed theoretical analysis of twisted plasma waves is also given.

Keywords: ponderomotive force; Laguerre-Gaussian; orbital angular momentum; plasma wave; self-generated magnetic field

CLC number: O534+.1

Document code: A

1 Introduction

High-power laser interactions with plasma have been widely studied since the 1970s. Most of these studies and applications are related to energy and momentum coupling from laser to plasma. Applications include particle accelerators^[1], X-ray sources, inertial confinement fusion, etc. Plasma waves are an important collective effect driven by high-power laser pulses. Energy and momentum are proven to be exchanged with high efficiency between charged particles and the field (laser or plasma field) in this process, which are the foundations of many applications. For example, the self-generated magnetic field plays an important role in laser-plasma interactions. The inverse Faraday (IF) effect for circularly polarized (CP) light^[2-5] is one of the well-known methods of laser-driven direct current magnetic field generation. This can be explained as the result of spin angular momentum (SAM) transfer from light to plasma. For a CP light beam, every photon has a SAM of \hbar . Here, $\sigma = \pm 1$ are for the right and left circular polarizations. On the other hand, light can also possess orbital angular momentum (OAM)^[6] and thereby have the potential to create plasmas with OAM. The OAM of a photon is due to the helical wavefront instead of the circular polarization. Mathematically, we can use a basis set of orthogonal Laguerre-Gaussian (LG) modes to express any helical wavefronts. For one pure LG mode with a twist index of l , every photon has $l\hbar$ of OAM. While such twisted light in conventional optics at low intensities has been widely studied (e.g., light tweezers^[7]), high-intensity ($I > 10^{16}$ W/cm²) twisted light has received moderate attention very recently. Unavoidably, the interaction medium will be plasma. Various new simulation phenomena and theories on interactions between intense

LG mode laser beams and plasma have been proposed^[8-22]. In experiments, several works have been reported^[16, 23-28]. However, high-efficiency OAM exchange between the plasma and field still needs more attention.

In previous work^[29], electron plasma waves with a helical rotating structure and static, axial magnetic field generation were confirmed using three-dimensional particle-in-cell (PIC) simulations. Now, we will give a general theory and more details under the condition of paraxial approximation where the spot size of the laser beam is large enough. The ponderomotive force of beating OAM lasers will be analyzed first. Then, the electrons will be driven to oscillate in a way to generate a twisted electron density. The associated axial magnetic field will be calculated using general theory and compared with the simulation results. Studies on the damping of twisted plasma waves and the axial magnetic field have been published in Refs. [21, 30, 31]. This paper is organized as follows: in Section 2, we demonstrate the ponderomotive potential for two beating LG laser pulses and one LG laser pulse. Both of them are different from the ponderomotive potential of a Gaussian pulse. In Section 3, we show the electric field, the helical electron density, and the magnetic field generation of twisted plasma waves in simulations. In Section 4, we give a general theory of twisted plasma waves driven by the beating of two LG beams. The helical electron density and the magnetic field are accurately described in theory. In Section 5, we explore the scheme of using the beating of an LG beam and a Gaussian beam.

2 The twisted ponderomotive potential using two beating LG-CP laser pulses

It is convenient to write down a Laguerre-Gaussian (LG)

transverse electromagnetic field with polarisation vector \hat{e}_s in cylindrical coordinates (r, θ, x) as

$$\mathbf{E} = \hat{e}_s \sum_{p,l} E_{p,l} F_{p,l}(X) \exp\left(ikx - i\omega t + il\theta - i\phi_{p,l} - \frac{ikw_b^2(x)X^2}{4f(x)}\right) + \text{c.c.}, \quad (1)$$

with the eigenfunction $F_{p,l}(X)$ given as $F_{p,l}(X) = C_{p,l} X^{|l|/2} e^{-X^2/2} L_p^l(X)$ where the normalized radial coordinate $X = 2r^2/w^2(x)$ is specified, $L_p^l(X)$ is a Laguerre polynomial with $C_{p,l} = \sqrt{2p!/[p!(p+|l|)!]}$ ($C_{0,1} = \sqrt{2/\pi} \approx 0.8$) being a normalisation to ensure an orthonormal set, the gouy phase $\phi_{p,l} = (2p+l+1)\arctan(x/x_R)$ and front surface curvature $f(x) = x + x_R^2/x$, the beam width $w_b(x) = w_{b,0} \sqrt{1 + x^2/x_R^2}$ and $w_{b,0} = w_b(0)$, the Rayleigh range is $x_R = kw_{b,0}^2$. For the following analysis, we simplify it by only considering the region within the Rayleigh range so that terms with $f(x)$ and $\phi_{p,l}$ can be ignored and we consider $w_b(x) = w_{b,0}$. Now we have an electric field from the laser as $\mathbf{E} = \hat{e}_s \sum_{p,l} E_{p,l} F_{p,l}(X) \exp(ikx - i\omega t + il\theta)$.

In the context of the discussions about the OAM of light, the multiplier term of $\exp(-il\theta)$ in Eq. (1) is the most significant one. It sets the twist of the wavefronts and determines the OAM of a mode. The OAM per photon for this mode is $l\hbar$, where l is the twist index. The laser pulse can efficiently exchange OAM with a structured target upon reflection^[8], but the same cannot be said about a helical pulse propagating through a uniform plasma. This can be illustrated by examining the direction of the ponderomotive force induced by a helical beam with electric field amplitude \mathbf{E} and frequency ω on plasma electrons,

$$\mathbf{F}_{\text{pond}} = -\nabla\Phi_{\text{pond}}, \quad \Phi_{\text{pond}} = \frac{e^2}{4m_e\omega^2} |\mathbf{E}(\mathbf{r}, t)|^2, \quad (2)$$

where Φ_{pond} is the ponderomotive potential and e and m_e are the electron charge and mass, respectively. The intensity of $|\mathbf{E}|^2$ is independent of θ and it follows from Eq. (2) that Φ_{pond} has no dependence on θ (see Fig. 1a). Therefore, the ponderomotive force \mathbf{F}_{pond} of a single LG beam has only a radial component in the cross section of the beam and it induces no azimuthal rotation of the plasma. The ponderomotive force is nonlinear, so the discussed difficulty can be overcome by using two co-propagating LG modes with different frequencies and twist indices to generate a ponderomotive force with a substantial azimuthal component.

We illustrate this for a pair of LG waves that have $p = 0$

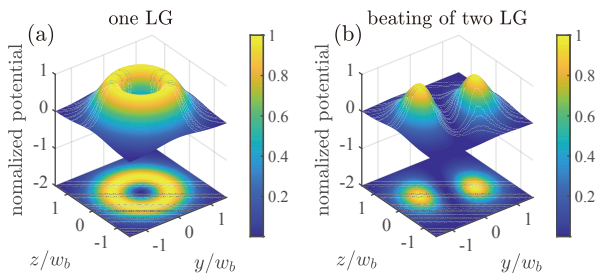


Fig. 1. Structure of the ponderomotive potential Φ_{pond} (in a. u.) of one LG laser pulse (a) and two beating LG laser pulses (b) in transverse plane (y - z). The ponderomotive force $\mathbf{F}_{\text{pond}} = -\nabla\Phi_{\text{pond}}$ has an azimuthal component only for two beating waves.

and opposite twist indices, $l_1 = -l_2 = l$, so that they have the same radial dependence. The waves are beating with slightly different frequencies: $\omega_1 = \omega_0$ and $\omega_2 = \omega_0 - \Delta\omega$, where $\Delta\omega \ll \omega_0$. We keep the radial normalization equivalent for all modes such that the real part of the final electric field looks like:

$$\mathbf{E} = \hat{e}_s E_0 F_{p,l}(X) [\cos(k_1 x - \omega_1 t - l\theta) + \cos(k_2 x - \omega_2 t + l\theta)]. \quad (3)$$

Considering an average over the timescale $t_{\text{fast}} = 2\pi/(\omega_1 + \omega_2)$ and length scale $x_{\text{fast}} = 2\pi/(k_1 + k_2)$, we have a slowly varying electric field of the form:

$$\mathbf{E}_{\text{slow}} = \hat{e}_s 2E_0 F_{p,l}(X) \cos\left(-\frac{\Delta k x}{2} + \frac{\Delta\omega t}{2} + l\theta\right), \quad (4)$$

where $\Delta k = k_1 - k_2$. This slowly varying envelope of the total electric field retains all of the angular momentum of the two combined waves. It is worth mentioning that the wave travels in the same direction as the sum of its parts, despite the sign change in k . To find the ponderomotive force we use the relation:

$$\mathbf{F}_{\text{pond}} = -\frac{e^2}{4m_e\omega^2} \nabla(E^2) = -\frac{e^2 E_0^2}{2m_e\omega_0^2} \nabla\left[F_{p,l}^2(X)(1 + \cos(-\Delta k x + \Delta\omega t + 2l\theta))\right]. \quad (5)$$

Putting $a_0 = eE_0/(m_e\omega_0 c)$, the ponderomotive potential can be described as

$$\Phi_{\text{pond}} = 0.5m_e c^2 a_0^2 F_{p,l}^2(X)(1 + \cos(-\Delta k x + \Delta\omega t + 2l\theta)). \quad (6)$$

The ponderomotive potential is then no longer cylindrically symmetric (see Fig. 1b). The resulting ponderomotive force, $\mathbf{F}_{\text{pond}} = -\nabla\Phi_{\text{pond}}$, has an azimuthal component and slowly rotates in the cross section of the propagating beams, i.e., in the y - z plane. In contrast, \mathbf{F}_{pond} produced by a superposition of conventional beams without OAM ($l = 0$) has no azimuthal component. The remainder of this work will elucidate twisted plasma waves driven by the twisted ponderomotive force and axial magnetic field generation related to the axial OAM carried by electrons.

3 Simulation results driven by twisted ponderomotive force

Using EPOCH^[32], we performed three-dimensional PIC simulations on the interactions between two beating LG-CP beams and plasma. For two LG-CP beams ($p = 0$), we choose the $l + \sigma = 0$ to get zero angular momentum. Therefore, magnetic field generation due to the IF effect is excluded. Some key simulation parameters are summarized in Table 1. The two LG-CP beams have frequencies and twist indices of $\omega_1 = \omega_0$, $\omega_2 = 0.9\omega_0$ and $l_1 = -1$, $l_2 = +1$, respectively. The frequency difference is set as the same as the plasma frequency $\omega_p = 0.1\omega_0$. $\omega_p = \sqrt{4\pi n_0 e^2/m_e}$ is the plasma frequency, where n_0 is the electron density and ω_0 is the frequency of beam 1 with a wavelength of $0.8 \mu\text{m}$. The target is initially set as a fully ionized hydrogen plasma with uniform density $n_0 = 4.5 \times 10^{18} \text{ cm}^{-3}$ and zero temperature. Both the incident pulses have a Gaussian shape with a total duration of $\tau_g = 200$ fs and a beam width of $w_b = 10 \mu\text{m}$, and the electric field

Table 1. 3D PIC simulation parameters. $n_c=1.8 \times 10^{21} \text{ cm}^{-3}$ is the critical density corresponding to the laser wavelength $0.8 \mu\text{m}$.

Laser parameters	LG-CP beam1	LG-CP beam 2
Electric field amplitude (E_{pl})	$E_{1(y,z)} = 1.0 \text{ TV/m}$	$E_{2(y,z)} = 1.0 \text{ TV/m}$
Wavelength	$\lambda_1 = 0.8 \mu\text{m}$	$\lambda_2 = 0.89 \mu\text{m}$
Twist index	$l_1 = -1$	$l_2 = 1$
Pulse duration (Gaussian shape)	$\tau_g = 200 \text{ fs}$ (75 cycles)	$\tau_g = 200 \text{ fs}$ (67.4 cycles)
Focal spot size ($1/e$ electric field)	$w_b = 10 \mu\text{m}$	$w_b = 10 \mu\text{m}$
Laser propagation direction	$+x$	$+x$
Other parameters		
Electron density	$n_e = 0.01 n_c$	
Simulation box ($x \times y \times z$)	$30 \mu\text{m} \times 50 \mu\text{m} \times 50 \mu\text{m}$	
Cell number ($x \times y \times z$)	$600 \times 800 \times 800$	
Macroparticles per cell for each species	2	

amplitude of $E_{y,z} = 1.0 \text{ TV/m}$. For the beam 1, the corresponding peak dimensionless vector potential of $a_0 = 0.25$.

In the following, we will give the main simulation results. The twisted electric field (E_r, E_θ, E_x) distributions are shown in Fig. 2. We should note that the non-zero distribution of E_θ (see Fig. 2b) clearly shows twist characteristics, which do not exist in normal longitudinal plasma waves. Furthermore, we find that the phase distributions of E_r (see Fig. 2a) and E_x (see Fig. 2c) are twisted with azimuth θ . These are different compared to longitudinal plasma waves driven by the beating of two Gaussian beams where there would be no dependence on θ ^[33]. Of particular note are the twisted electron density perturbations δn_e presented in Fig. 3a and a static axial magnetic field B_x in the y - z plane, shown in Fig. 3c. The magnetic field can be as high as 8 T and persists for hundreds of femtoseconds after the laser beams pass by. We also observe an azimuthal magnetic field distribution which is presented in Fig. 3e. The dashed lines on the right of Fig. 3 are line-outs from the slices plotted against the position along the line-outs d plotted in the left of Fig. 3. As time passes, the twisted electron density rotates around the x -axis with angular frequency ω_{pe} . The scheme works for other choices of different twist indices (see 3D PIC simulation results in Section 5). There, twist effects using an LG and a Gaussian beam are confirmed and likely to be easier to realize experimentally. However, to simplify the theoretical analysis, we choose opposite twist indices in the following analysis. We also choose circularly polarized lasers instead of linearly polarized lasers to exclude the effects of polarization deflection due to the twisted electron density. The dependence of the polarization deflection on the laser frequency can lead to a symmetry break in the transverse plane. Frequency detuning effects should be discussed for a real experiment. Additional simulations have been accomplished with different beating frequencies. We found that the axial magnetic fields are in similar distributions although a weaker peak amplitude ($\approx 90\%$) when the beating frequency is $\Delta\omega = (1.00 \pm 0.05)\omega_p$.

4 The general theory of twisted plasma waves driven by twisted ponderomotive force

First, we solve the non-relativistic cold electron-fluid equa-

tions driven by the twisted ponderomotive force in Section 2.

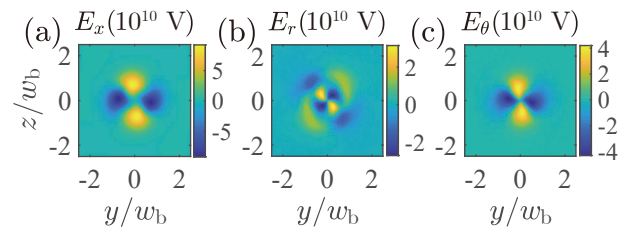


Fig. 2. 3D PIC simulation results of electric field and fluid velocity distribution at transverse plane (y - z plane) at the centre of simulation box ($x = 15 \mu\text{m}$) and the time 320 fs after the laser has passed by. (a), (b), and (c) show transverse slices of E_x, E_θ , and E_r .

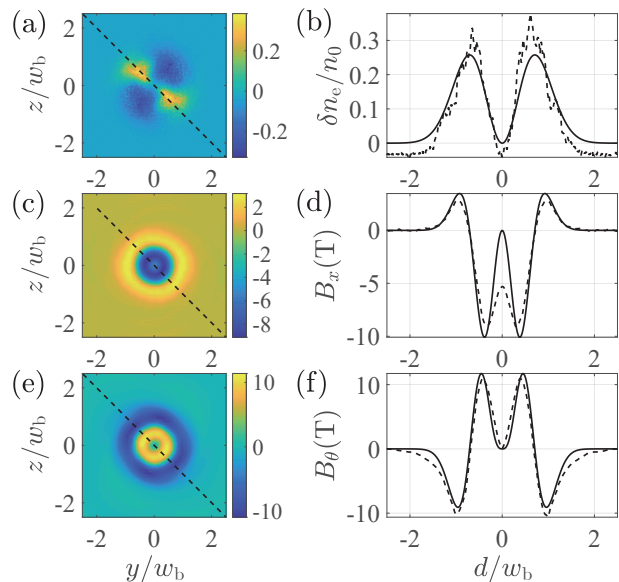


Fig. 3. PIC results of transverse profile of (a) electron density perturbation δn_e , (c) axial magnetic field B_x and (e) azimuthal magnetic field B_θ at the centre of simulation box ($x = 15 \mu\text{m}$) and the time 320 fs after the laser has passed by. The dashed lines shown in the transverse slices are the line outs used to plot the graphics on the right. The plots on the right, (b), (d), and (f), are line outs from the slices plotted against the position along the line outs d plotted in (a), (c), and (e). d is the coordinate along the dashed lines. Solid lines in (b), (d) and (f) are theory predictions, for the same situation considered in Table 1.

Using linear fluid theory (LFT)^[32], we can describe laser-driven electron plasma waves as

$$\begin{cases} m_e \partial_t \mathbf{u} = e \nabla \Phi + \mathbf{F}_{\text{pond}} \\ \partial_t \delta n_e + n_0 \nabla \cdot \mathbf{u} = 0 \\ \nabla^2 \Phi = 4\pi e \delta n_e \end{cases} \quad (7)$$

Here, ions are assumed to be immobile, and δn_e is the difference between the electron density n_e and ion density n_0 . \mathbf{u} is the velocity of the electron fluid and Φ is the static electric

$$\begin{cases} r^{-2} \partial_\theta^2 \Phi_{\text{pond}} = -4a_0^2 l^2 / (X w_b^2) F_{p,l}^2(X) \cos(-\Delta kx + \Delta \omega t + 2l\theta) \\ r^{-1} \partial_r (r \partial_r) \Phi_{\text{pond}} = 4(a_0^2 / w_b^2) [(F_{p,l}^2(X))' + X(F_{p,l}^2(X))''] [1 + \cos(-\Delta kx + \Delta \omega t + 2l\theta)] \\ \partial_x^2 \Phi_{\text{pond}} = -0.5 \Delta k^2 a_0^2 F_{p,l}^2(X) \cos(-\Delta kx + \Delta \omega t + 2l\theta) \end{cases}$$

With a definition of $G_{p,l}(X)$,

$$G_{p,l}(X) = \frac{(F_{p,l}^2(X))' + X(F_{p,l}^2(X))''}{F_{p,l}^2(X)}, \quad (9)$$

we can write $\nabla^2 \Phi_{\text{pond}}$ as

$$\nabla^2 \Phi_{\text{pond}} = \frac{a_0^2}{2} F_{p,l}^2(X) \left[-\Delta k^2 - \frac{8l^2}{X w_b^2} + \frac{8}{w_b^2} G_{p,l}(X) \right] \cos(-\Delta kx + \Delta \omega t + 2l\theta) + \frac{4a_0^2}{w_b^2} F_{p,l}^2(X) G_{p,l}(X). \quad (10)$$

We will only consider the part with the cosine which will drive our forced plasma oscillation. When the ponderomotive force drives the perturbations with a frequency equal to $\Delta \omega = \omega_{pe}$, we have a solution of δn_e as

$$\begin{aligned} \frac{\delta n_e}{n_0} &= \frac{\tau c^2 \Delta k^2 a_0^2}{4\omega_p} \Xi_{p,l}(X) \sin(-\Delta kx + \omega_{pe} t + 2l\theta), \\ \Xi_{p,l}(X) &= F_{p,l}^2(X) \left[1 + \frac{1}{\Delta k^2 w_b^2} \frac{8l^2}{X} - \frac{8}{\Delta k^2 w_b^2} G_{p,l}(X) \right]. \end{aligned} \quad (11)$$

It suggests a linearly growing amplitude with the laser pulse duration τ . Our simulation use two LG-CP beams having same parameters except different wavelengths and twist indexes ($p=0, l_1=-l_2=l$). The function of $\Xi_{p,l}(X)$ electron density perturbation can be presented in the following explicit form,

$$\Xi_{p,l}(X) = F_{0,l}^2(X) \left[1 + \frac{8}{\Delta k^2 w_b^2} (-X + 1 + 2|l|) \right]. \quad (12)$$

It is the same result as the Eq. (2) in Ref. [28]. If $1/\Delta k^2 w_b^2$ is small then $\Xi_{p,l}(X) = F_{p,l}^2(X)$ for simple cases, and for cases where $p=0$ then $\Xi_{0,l}(X) = C_{0l} X^{|l|} e^{-X}/|l|!$, this can calculate a situation for a Gaussian wave where $l=0$ so that $\Xi_{0,0}(X) = e^{-X}$. In this paper, we will focus on the case of paraxial approximation with small $1/\Delta k^2 w_b^2$.

In a similar way, the electric field \mathbf{E} and the velocity field \mathbf{u} can be solved in the following equations:

$$\begin{cases} \partial_t^2 \mathbf{E} + \omega_{pe}^2 \mathbf{E} = -\omega_{pe}^2 \mathbf{F}_{\text{pond}} / e \\ \partial_t^2 \mathbf{u} + \omega_{pe}^2 \mathbf{u} = \partial_t \mathbf{F}_{\text{pond}} / m_e \end{cases}, \quad (13)$$

According to the Eq. (5), the force is

potential. The resulting equation for the perturbations of electron density δn_e in a plasma with an initially uniform electron density n_0 has the form

$$\partial_t^2 \delta n_e + \omega_{pe}^2 \delta n_e = \frac{n_0}{m_e} \nabla \cdot \mathbf{F}_{\text{pond}}. \quad (8)$$

This equation is analogous to the equation that describes a driven harmonic oscillator. The driving item can be calculated as

$$\begin{cases} F_{\text{pond},\theta} = (lc^2 a_0^2 m_e / w_b) \sqrt{2/X} F_{p,l}^2(X) \sin(-\Delta kx + \Delta \omega t + 2l\theta) \\ F_{\text{pond},r} = -(c^2 a_0^2 m_e / w_b) \sqrt{2X} (F_{p,l}^2(X))' \cos(-\Delta kx + \Delta \omega t + 2l\theta) \\ F_{\text{pond},x} = -0.5(c^2 a_0^2 m_e \Delta k) F_{p,l}^2(X) \sin(-\Delta kx + \Delta \omega t + 2l\theta) \end{cases} \quad (14)$$

We can ignore the last part of the constant force in the radial direction. For the velocity we can again neglect the constant radial term giving $\partial_t F$ as,

$$\begin{cases} \partial_t F_{\text{pond},\theta} = (lc^2 a_0^2 m_e \omega_{pe} / w_b) \sqrt{2/X} F_{p,l}^2(X) \cos(-\Delta kx + \Delta \omega t + 2l\theta) \\ \partial_t F_{\text{pond},r} = (c^2 a_0^2 m_e \omega_{pe} / w_b) \sqrt{2X} (F_{p,l}^2(X))' \sin(-\Delta kx + \Delta \omega t + 2l\theta) \\ \partial_t F_{\text{pond},x} = -0.5(c^2 a_0^2 m_e \omega_{pe} \Delta k) F_{p,l}^2(X) \cos(-\Delta kx + \Delta \omega t + 2l\theta) \end{cases} \quad (15)$$

Mirroring the approach used above, the electric field and fluid velocity are found to be

$$\begin{cases} E_\theta = -0.5 \tau \omega_{pe} lc^2 a_0^2 (m_e / e / w_b) \sqrt{2/X} F_{p,l}^2(X) \cos(-\Delta kx + \Delta \omega t + 2l\theta) \\ E_r = -\tau \omega_{pe} (c^2 a_0^2 m_e / e / w_b) \sqrt{X/2} (F_{p,l}^2(X))' \sin(-\Delta kx + \Delta \omega t + 2l\theta) \\ E_x = 0.25 \tau \omega_{pe} c^2 a_0^2 (m_e / e) \Delta k F_{p,l}^2(X) \cos(-\Delta kx + \Delta \omega t + 2l\theta) \end{cases}, \quad (16)$$

and

$$\begin{cases} u_\theta = -0.5(lc^2 a_0^2 \tau / w_b) \sqrt{2/X} F_{p,l}^2(X) \sin(-\Delta kx + \Delta \omega t + 2l\theta) \\ u_r = (c^2 a_0^2 \tau / w_b) \sqrt{X/2} (F_{p,l}^2(X))' \cos(-\Delta kx + \Delta \omega t + 2l\theta) \\ u_x = 0.25(c^2 a_0^2 \tau \Delta k) F_{p,l}^2(X) \sin(-\Delta kx + \Delta \omega t + 2l\theta) \end{cases} \quad (17)$$

Using the explicit form of $(F_{0,l}^2(X))' = (|l|/X - 1)F_{0,l}^2$, we can get the same result as Eq. (s7) and Eq. (s8) in the supplemental material of Ref. [29].

In the theory above, the electric current density is $\mathbf{j}^e = -en_0 \mathbf{u}$, and the displacement current density is $\mathbf{j}^{\text{dis}} = \partial \mathbf{E} / (4\pi \partial t)$. According to high-order fluid theory^[34,35], the second-order current can generate a magnetic field even though $\mathbf{j}^e + \mathbf{j}^{\text{dis}} = 0$ in the first order. In the PIC simulation results, the time-averaged net current in both the azimuthal directions $\langle j_\theta^{(2)} \rangle$ (i.e., net rotating current) and the axial direction $\langle j_x^{(2)} \rangle$ are confirmed. With a definition of $\tilde{j}_0 = -en_0 \tau^2 c^4 \Delta k^3 a_0^4 / \omega_p$, the second-order current is

$$\begin{cases} j_\theta^{(2)} = -(l/8) \tilde{j}_0 / (w_b \Delta k) \sqrt{2/X} F_{p,l}^4(X) \sin^2(-\Delta kx + \Delta \omega t + 2l\theta) \\ j_r^{(2)} = (1/8) \tilde{j}_0 / (w_b \Delta k) \sqrt{X/2} (F_{p,l}^2(X))' F_{p,l}^2(X) \sin 2(-\Delta kx + \Delta \omega t + 2l\theta) \\ j_x^{(2)} = (1/16) \tilde{j}_0 F_{p,l}^4(X) \sin^2(-\Delta kx + \Delta \omega t + 2l\theta) \end{cases} \quad (18)$$

The equation for the second-order vector potential $A^{(2)}$ can be

written as

$$(\partial_t^2 - c^2 \nabla^2 + \omega_{pe}^2) \mathbf{A}^{(2)} = 4\pi c \mathbf{j}^{(2)}. \quad (19)$$

$$\begin{cases} A_\theta^{(2)} = -(l\pi c/4) \tilde{j}_0 / (w_b \Delta k) \sqrt{2/X} F_{p,l}^4(X) \left[\frac{1}{\Delta \omega^2} - \frac{1}{4\Delta k^2 c^2 - 3\Delta \omega^2} \cos 2(-\Delta kx + \Delta \omega t + 2l\theta) \right] \\ A_r^{(2)} = (\pi c/2) \tilde{j}_0 / (w_b \Delta k) \sqrt{X/2} (F_{p,l}^2(X))^y F_{p,l}^2(X) \frac{1}{4\Delta k^2 c^2 - 3\Delta \omega^2} \sin 2(-\Delta kx + \Delta \omega t + 2l\theta) \\ A_x^{(2)} = (\pi c/8) \tilde{j}_0 F_{p,l}^4(X) \left[\frac{1}{\Delta \omega^2} - \frac{1}{4\Delta k^2 c^2 - 3\Delta \omega^2} \cos 2(-\Delta kx + \Delta \omega t + 2l\theta) \right] \end{cases} \quad (20)$$

The axial and azimuthal components contain a constant term and a second harmonic oscillating term. However, the radial component has only a second harmonic oscillating term. The quasi-stationary magnetic field can be calculated by $\mathbf{B} = \nabla \times \mathbf{A}^{(2)}$,

$$\begin{cases} B_r = \frac{1}{r} \frac{\partial A_x^{(2)}}{\partial \theta} - \frac{\partial A_\theta^{(2)}}{\partial x} = 0 \\ B_\theta = -\frac{\partial A_x^{(2)}}{\partial r} = -\frac{\pi c \tilde{j}_0}{2\sqrt{2} w_b \Delta \omega^2} \sqrt{X} (F_{p,l}^4)^y \\ B_x = \frac{1}{r} \frac{\partial r A_\theta^{(2)}}{\partial r} = -\frac{l\pi c \tilde{j}_0}{w_b^2 \Delta \omega^2 \Delta k} (F_{p,l}^4)^y \end{cases} \quad (21)$$

The relationship between the azimuthal and axial components is $B_\theta/B_x = 0.25(w_b \Delta k/l) \sqrt{X}$. With the parameters of $\kappa_w = \Delta k w_b$ and $\kappa_n = \tau c^2 \Delta k^2 a_0^2 / (4\omega_p)$, we can get the amplitude of B_x ,

$$B_{x0} = -\frac{l\pi c \tilde{j}_0}{w_b^2 \Delta \omega^2 \Delta k} = 8lc \sqrt{\pi m_e n_0} \left(\frac{\kappa_n}{\kappa_w}\right)^2. \quad (22)$$

If we have $\kappa_w = 10$, $\kappa_n = 0.1$ and $\tilde{n}_0 = n_0/n_c$, we can get $B_{x0}(T) \sim 5l\sqrt{\tilde{n}_0}$. It means that if we assume that the electron density perturbation is small and the paraxial approximation works well, the amplitude of B_x will increase with a larger plasma density. Since the plasma density cannot be overdense in our scheme here, we expect that there is an upper limit on the amplitude of B_x .

In the PIC simulation shown in Table 1, Fig. 2 and Fig. 3 give the results. Here, $1/w_b^2 \Delta k^2 = 0.016$ when we use $\Delta k = \omega_{pe}/c$. For simplicity, Eq. (11) has been obtained assuming a flat-top pulse with duration τ . For the truncated Gaussian pulse used in the PIC simulation (i.e., $I(t) = 0$ for $|t - t_p| \geq \tau_g/2$ where $t_p = \tau_g/2$ is the time of peak intensity), $\tau = 0.75\tau_g$ is appropriate. The Eq. (16) shows that the radial field E_r is phase different compared to the azimuthal field E_θ and axial fields E_x . These are the same as the results in Fig. 2. The radial field u_r is also phase different compared to the azimuthal field u_θ and axial fields u_x according to Eq. (17). Both $u_\theta \propto l$ and $E_\theta \propto l$ show the importance of the OAM of the driving lasers. The calculation results of electron density perturbation in the transverse plane are shown as a solid line in Fig. 3b, which is close to the simulation result (dashed line). The difference is thought to be caused by ignoring the last part of the constant force in the radial direction in Eq. (10). Theoretical predictions of the magnetic field from Eq. (21) are shown as solid lines in Fig. 3d and f. They are also close to the dashed lines. The result of the LFT twisted plasma waves with a helical rotating structure. It is different from the

In the paraxial approximation where only the dominant axial derivative in the Laplacian term is accounted for, we can obtain the explicit expressions for the vector potential $\mathbf{A}^{(2)}$ as

longitudinal plasma waves driven by the beating of two Gaussian lasers, where transverse profiles depend only on radius^[33]. The magnetic field generation due to the second-order current is explained well in the paraxial approximation. While this study is limited to plasma waves with small amplitudes, the high-order terms are ignored in Eq. (7). In other simulations, we observed spiral phenomena that may be related to the high-order nonlinear terms.

To understand more details on the twisted plasma waves with electrons carrying axial OAM, we analyze the oscillating phase of a single electron under a transverse electric field of $E_r = E_{r1} \sin \Phi_0$ and $E_\theta = E_{\theta1} \cos \Phi_0$, where $\Phi_0 = \omega_p t + 2l\theta$ at $x = 0$ and θ_0 is the azimuth. Here, $E_r(r_0, \theta_0)$ and $E_\theta(r_0, \theta_0)$ are rewritten for our purpose according to Eq. (16). The solutions of the motion equation $m_e d^2 \mathbf{r}_1 / dt^2 = -e \mathbf{E}(t, \mathbf{r}_0)$ to the first order in coordinates of (y, z) are

$$\begin{cases} v_{y1} = (E_{r1} \cos \theta_0 \cos \Phi_0 + E_{\theta1} \sin \theta_0 \sin \Phi_0)(e/m_e \omega_p) \\ v_{z1} = (E_{r1} \sin \theta_0 \cos \Phi_0 - E_{\theta1} \cos \theta_0 \sin \Phi_0)(e/m_e \omega_p) \end{cases} \quad (23)$$

Within such an oscillating electric field, electrons will oscillate locally with an azimuthally dependent phase to the first order. The central shift velocity is assumed to be small and should have no contribution to the rotating phase ϕ . If the amplitude dependence on the radius is kept only for positive and negative values, the dependence of the rotating phase ϕ on azimuth θ_0 is

$$\phi = \arctan\left(\frac{v_{z1}}{v_{y1}}\right) = \begin{cases} \omega_p t + (2l+1)\theta_0, & r_0 < r_b \\ -\omega_p t - (2l-1)\theta_0, & r_0 > r_b \end{cases}, \quad (24)$$

where $r_b = w_b \sqrt{|l|/2}$ and $l = -1$. Furthermore, we can show that the rotating electron density in the transverse plane comes from particles oscillating elliptically in the transverse plane with an azimuthally dependent phase. We reconstruct the 2D electron density perturbation in the transverse plane to a higher-order approximation from particle oscillation. This oscillation can be viewed as a mapping of the r_0 space onto the $r_0 + r_1$ space. Here, we have $r_1 = \int (v_{y1}, v_{z1}) dt$. The mapping is assumed to be single-valued and regular here. Then, the number density due to the motion can be given by $ndV = n_0 dV_0$, where the two volume elements (dV_0 and dV) are related by the Jacobian of the transformation^[36]. From the electron oscillation, we can get

$$\frac{n_0}{n} = \frac{\partial(y_0 + y_1, z_0 + z_1)}{\partial(y_0, z_0)}. \quad (25)$$

The electron density can be approximated to second order

$$n \approx n_0 [1 + \tilde{n}_1(\eta, r_0) \sin \Phi_0 + o(\eta^2, r_0) + o(\eta^2, r_0) \cos 2\Phi_0],$$

$$\tilde{n}_1 = \frac{1}{\omega_p} (2l \frac{v_{\theta 1}}{r_0} + \frac{v_{r1}}{r_0} + \frac{dv_{r1}}{dr_0}). \quad (26)$$

Here, we get $v_{r1} = eE_{r1}/(m_e\omega_p)$ and $v_{\theta 1} = -eE_{\theta 1}/(m_e\omega_p)$ from Eq. (23). The explicit form of Eq. (26) shows that the first order electron density is the same as the LFT result of Eq. (11) in the transverse plane if we ignore $k_p x$. We can obtain the electric field in the azimuth component to a second order, $E_\theta = E_{\theta 1} \cos \Phi_0 + o(\eta^2, r_0) \sin 2\Phi_0$. To the first order, it is just the same as the electric field from LFT. We can write a demo with some randomly distributed particles rotating with a phase dependence of azimuth in the plane. The collected motion of rotation with a phase dependence of azimuth will create a rotating electron density and carry axial OAM. Such a rotating electron density in plasma will produce a twisted electrostatic field, which in reality can push every electron rotating with a phase dependence of azimuth. It is a self-consistency process in twisted plasma waves.

Finally, using the equation of $\langle L_x^c \rangle = -\langle j_\theta^2 \rangle r m_e / e$, we can get the theoretical result of the transverse profile of the time-averaged axial OAM density. The integration of $\langle L_x^c \rangle$ over radius r is not zero when $l \neq 0$. For electromagnetic fields, the energy and momentum of electromagnetic waves are transported essentially by electric and magnetic fields. But for the plasma wave fields, electrostatic waves in plasma carry energy but no momentum if we do not consider the magnetic field due to the high order effect. Only particles will carry axial momentum and OAM. The same results can also be found in Ref. [31]. In Refs. [30,31], Langmuir plasma waves carrying a finite OAM are studied using kinetic theory in the paraxial approximation. The dispersion relation and energy and momentum exchange between particles and the field in the damping process are studied for twisted plasma waves.

5 Simulation results driven by beating between an LG pulse and a Gaussian pulse

Considering the difficulties of producing high intensity LG beams in experiments, we accomplished a simulation using the beating of one LG beam ($l = -1$) and one Gaussian beam ($l = 0$). Now, the ponderomotive force is $F_{pond}(r, \theta, x, t) \propto \nabla \cos(\omega_p t - k_p x - \theta)$ and then the electron density perturbation is $\delta n_e \propto \sin(\omega_p t - k_p x - \theta)$. We set the beam 2 in Table 1 as a Gaussian beam and the other parameters are kept the same. Their frequency shift was also set to match the plasma frequency. Similar twisted electron density and magnetic field generation are observed in Fig. 4. Of particular note are the

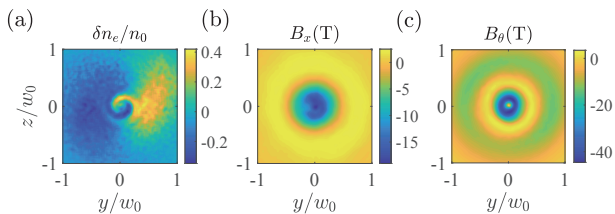


Fig. 4. PIC results of transverse profile of (a) electron density perturbation δn_e , (b) axial magnetic field B_x and (c) azimuthal magnetic field B_θ at the centre of simulation box ($x = 15 \mu\text{m}$) and the time 320 fs after the laser has passed by.

single helical electron density distribution δn_e presented in Fig. 4a. In Fig. 4b, the magnetic field can be as high as 20 T. In future experiments, we may consider using temporally-chirped pulses for twisted plasma wave excitation^[37]

6 Conclusions

In conclusion, twisted plasma waves carrying OAM are produced in PIC simulations by using beating of two LG beams or one LG and one Gaussian beam. We compare the ponderomotive force of two beating LG beams with the ponderomotive force of two beating Gaussian beams. The substantial azimuthal component of the ponderomotive force provides a unique tool for an effective exchange of OAM between the light and the plasma. Twisted electron plasma waves with a rotating helical structure are confirmed using three-dimensional PIC simulations. Once being excited, the twisted plasma wave can persist in the plasma long after the laser beams that create the ponderomotive force are gone. Essentially, the electrons are left oscillating along elliptical orbits in the transverse plane with an azimuthally dependent phase offset. This collectively yields a persistent, rotating wave structure, and an associated with it nonlinear electron current. The current configuration that is similar to that in a solenoid creates a longitudinal quasi-static magnetic field. Under the condition of paraxial approximation, we develop a general theory to explain the twist of the plasma waves and calculate the distributions of the magnetic fields in axial and azimuthal directions. Finally, to relax the experimental conditions of getting relativistic twisted laser intensities, we run simulations using beating between an LG and a Gaussian beam. The twisted ponderomotive force and twisted plasma waves would be easier to realize experimentally when only one beam with OAM is needed.

Data availability

The datasets generated and analyzed during the current study are available from the corresponding author on reasonable request.

Code availability

PIC simulations were performed with the fully relativistic open-access 3D PIC code EPOCH^[38].

Acknowledgements

This work was supported by USTC Research Funds of the Double First-Class Initiative (YD2140002003), Strategic Priority Research Program of CAS (XDA25010200), CAS Project for Young Scientists in Basic Research (YSBR060), and Newton International Fellows Alumni follow-on funding. Simulations were performed with EPOCH (developed under UK EPSRC Grants EP/G054950/1, EP/G056803/1, EP/G055165/1, and EP/M022463/1). The Computational Center of USTC and Hefei Advanced Computing Center are acknowledged for computational support.

Conflict of interest

The authors declare that they have no conflict of interest.

Preprint statement

Research presented in this work was posted on a preprint server prior to publication in *JUSTC*. The corresponding preprint article can be found here: arXiv: 2211.01630. <https://arxiv.org/abs/2211.01630>.

Biographies

Yin Shi received his Ph.D. degree from Shanghai Institute of Optics and Fine Mechanics (SIOM), CAS, in 2015. He is currently a Special Researcher at the University of Science and Technology of China. His research focuses on laser plasma interactions and high-energy-density physics.

References

- [1] Esarey E, Schroeder C B, Leemans W P. Physics of laser-driven plasma-based electron accelerators. *Reviews of Modern Physics*, **2009**, *81*: 1229–1285.
- [2] Ali S, Davies J R, Mendonca J T. Inverse Faraday effect with linearly polarized laser pulses. *Physical Review Letters*, **2010**, *105*: 035001.
- [3] Haines M G. Generation of an axial magnetic field from photon spin. *Physical Review Letters*, **2001**, *87*: 135005.
- [4] Najmudin Z, Tatarakis M, Pukhov A, et al. Measurements of the inverse Faraday effect from relativistic laser interactions with an underdense plasma. *Physical Review Letters*, **2001**, *87*: 215004.
- [5] Sheng Z M, Meyer-ter-Vehn J. Inverse Faraday effect and propagation of circularly polarized intense laser beams in plasmas. *Physical Review E, Statistical Physics, Plasmas, Fluids, and Related Interdisciplinary Topics*, **1996**, *54*: 1833–1842.
- [6] Allen L, Beijersbergen M W, Spreeuw R J, et al. Orbital angular momentum of light and the transformation of Laguerre-Gaussian laser modes. *Physical Review A, Atomic, Molecular, and Optical Physics*, **1992**, *45*: 8185–8189.
- [7] Yao A M, Padgett M J. Orbital angular momentum: Origins, behavior and applications. *Advances in Optics and Photonics*, **2011**, *3*: 161.
- [8] Shi Y, Shen B, Zhang L, et al. Light fan driven by a relativistic laser pulse. *Physical Review Letters*, **2014**, *112*: 235001.
- [9] Vieira J, Trines R M, Alves E P, et al. High orbital angular momentum harmonic generation. *Physical Review Letters*, **2016**, *117*: 265001.
- [10] Zhang L, Shen B, Zhang X, et al. Deflection of a reflected intense vortex laser beam. *Physical Review Letters*, **2016**, *117*: 113904.
- [11] Zhang X, Shen B, Shi Y, et al. Generation of intense high-order vortex harmonics. *Physical Review Letters*, **2015**, *114*: 173901.
- [12] Vieira J, Mendonça J T. Nonlinear laser driven donut wakefields for positron and electron acceleration. *Physical Review Letters*, **2014**, *112*: 215001.
- [13] Wang W, Shen B, Zhang X, et al. Hollow screw-like drill in plasma using an intense Laguerre-Gaussian laser. *Scientific Reports*, **2015**, *5*: 8274.
- [14] Zhang X, Shen B, Zhang L, et al. Proton acceleration in underdense plasma by ultraintense Laguerre-Gaussian laser pulse. *New Journal of Physics*, **2014**, *16*: 123051.
- [15] Vieira J, Mendonça J T, Quéré F. Optical control of the topology of laser-plasma accelerators. *Physical Review Letters*, **2018**, *121*: 054801.
- [16] Longman A, Fedosejevs R. Mode conversion efficiency to Laguerre-Gaussian OAM modes using spiral phase optics. *Optics Express*, **2017**, *25*: 17382–17392.
- [17] Ju L B, Zhou C T, Jiang K, et al. Manipulating the topological structure of ultrarelativistic electron beams using Laguerre-Gaussian laser pulse. *New Journal of Physics*, **2018**, *20*: 063004.
- [18] Zhu X L, Chen M, Weng S M, et al. Single-cycle terawatt twisted-light pulses at midinfrared wavelengths above 10 μm . *Physical Review Applied*, **2019**, *12*: 054024.
- [19] Tikhonchuk V T, Korneev P, Dmitriev E, et al. Numerical study of momentum and energy transfer in the interaction of a laser pulse carrying orbital angular momentum with electrons. *High Energy Density Physics*, **2020**, *37*: 100863.
- [20] Nuter R, Korneev P, Thiele I, et al. Plasma solenoid driven by a laser beam carrying an orbital angular momentum. *Physical Review E*, **2018**, *98*: 033211.
- [21] Blackman D R, Nuter R, Korneev P, et al. Nonlinear Landau damping of plasma waves with orbital angular momentum. *Physical Review E*, **2020**, *102*: 033208.
- [22] Longman A, Fedosejevs R. Kilo-Tesla axial magnetic field generation with high intensity spin and orbital angular momentum beams. *Physical Review Research*, **2021**, *3*: 043180.
- [23] Leblanc A, Denoëud A, Chopineau L, et al. Plasma holograms for ultrahigh-intensity optics. *Nature Physics*, **2017**, *13*: 440–443.
- [24] Denoëud A, Chopineau L, Leblanc A, et al. Interaction of ultraintense laser vortices with plasma mirrors. *Physical Review Letters*, **2017**, *118*: 033902.
- [25] Longman A, Salgado C, Zeraoui G, et al. Off-axis spiral phase mirrors for generating high-intensity optical vortices. *Optics Letters*, **2020**, *45*: 2187–2190.
- [26] Bae J Y, Jeon C, Pae K H, et al. Generation of low-order Laguerre-Gaussian beams using hybrid-machined reflective spiral phase plates for intense laser-plasma interactions. *Results in Physics*, **2020**, *19*: 103499.
- [27] Aboushelbaya R, Glize K, Savin A F, et al. Measuring the orbital angular momentum of high-power laser pulses. *Physics of Plasmas*, **2020**, *27*: 053107.
- [28] Zeng X, Zheng S, Cai Y, et al. Generation and imaging of a tunable ultrafast intensity-rotating optical field with a cycle down to femtosecond region. *High Power Laser Science and Engineering*, **2020**, *8*: e3.
- [29] Shi Y, Vieira J, Trines R M G M, et al. Magnetic field generation in plasma waves driven by copropagating intense twisted lasers. *Physical Review Letters*, **2018**, *121*: 145002.
- [30] Blackman D R, Nuter R, Korneev P, et al. Kinetic plasma waves carrying orbital angular momentum. *Physical Review E*, **2019**, *100*: 013204.
- [31] Blackman D R, Nuter R, Korneev P, et al. Twisted kinetic plasma waves. *Journal of Russian Laser Research*, **2019**, *40*: 419–428.
- [32] Arber T D, Bennett K, Brady C S, et al. Contemporary particle-in-cell approach to laser-plasma modelling. *Plasma Physics and Controlled Fusion*, **2015**, *57*: 113001.
- [33] Fedele R, de Angelis U, Katsouleas T. Generation of radial fields in the beat-wave accelerator for Gaussian pump profiles. *Physical Review A, General Physics*, **1986**, *33*: 4412–4414.
- [34] Gorbunov L, Mora P, Antonsen T M Jr. Magnetic field of a plasma wake driven by a laser pulse. *Physical Review Letters*, **1996**, *76*: 2495–2498.
- [35] Gorbunov L M, Mora P, Antonsen T M. Quasistatic magnetic field generated by a short laser pulse in an underdense plasma. *Physics of Plasmas*, **1997**, *4*: 4358–4368.
- [36] Dawson J M. Nonlinear electron oscillations in a cold plasma. *Physical Review*, **1959**, *113*: 383–387.
- [37] Cowley J, Thornton C, Arran C, et al. Excitation and control of plasma wakefields by multiple laser pulses. *Physical Review Letters*, **2017**, *119*: 044802.
- [38] EPOCH Particle-In-Cell code for plasma simulations. <https://github.com/epochpic/epochpic.github.io>. Accessed April 10, 2022.